



**Interlayer Mixing in Lithium Nickel Manganese  
Cobalt Oxide Cathode Materials for Rechargeable  
Lithium Batteries**

by

**TAN TZE QING  
(1330410909)**

A thesis submitted in fulfilment of the requirements for the degree of  
Master of Science (Materials Engineering)

**School of Materials Engineering  
UNIVERSITI MALAYSIA PERLIS**

2014

# UNIVERSITI MALAYSIA PERLIS

## DECLARATION OF THESIS

Author's full name : TAN TZE QING  
Date of birth : 28 JULY 1988  
Title : Interlayer Mixing in Lithium Nickel Manganese Cobalt Oxide  
Cathode Materials for Rechargeable Lithium Batteries  
Academic Session : 2012 / 2013

I hereby declare that the thesis becomes the property of Universiti Malaysia Perlis (UniMAP) and to be placed at the library of UniMAP. This thesis is classified as :

- CONFIDENTIAL** (Contains confidential information under the Official Secret Act 1972)\*
- RESTRICTED** (Contains restricted information as specified by the organization where research was done)
- OPEN ACCESS** I agree that my thesis is to be made immediately available as hard copy or on-line open access (full text)

I, the author, give permission to the UniMAP to reproduce this thesis in whole or in part for the purpose of research or academic exchange only (except during a period of \_\_\_\_ years, if so requested above).

Certified by:

SIGNATURE

880728-35-5102

(NEW IC NO. / PASSPORT NO.)

Date : 25 AUG 2014

SIGNATURE OF SUPERVISOR

DR. MOHD SOBRI IDRIS

NAME OF SUPERVISOR

Date : 25<sup>th</sup> AUGUST 2014

**NOTES :** \* If the thesis is CONFIDENTIAL or RESTRICTED, please attach with the letter from the organization with period and reasons for confidentiality or restriction.

## ACKNOWLEDGEMENTS

I would like to express my sincere gratitude and deepest appreciation to my supervisor Dr. Mohd Sobri Idris for giving me the opportunity to work under his supervision. I am very thankful that he shared his knowledge especially in X-ray diffraction field and Rietveld refinement. I am also very grateful for his support and guidance throughout the research project for about two years. He has been a great mentor and always gives a lot of advises during discussion. The patience and encouragement that he has given to me throughout the project are very much appreciated. I am also very grateful for the experience and knowledge shared by Dr. Rozana Aina Maulat Osman and Professor Dr. Azmi Rahmat.

Besides that, I would like to thank to all my friends in Universiti Malaysia Perlis especially Ms. Toh Guat Yee for their co-operation and assistance given that smoothen my research project. Because of them, my time as a postgraduate student becomes very meaningful and valuable. Special thanks to Mr. Soo Soon Peng for giving me valuable suggestions and helpful opinions towards my study.

I would like to devote deepest thanks to all the staffs of School of Materials Engineering especially all the lab technicians, Mr. Mohammed Faisal Rusli, Mr. Mohd Nasir Bin Haji Ibrahim, Mr. Ku Hasrin Ku Bin Abdul Rahman and Mr. Muhamad Hafiz Bin Zan@Hazizi in contributing the efforts, commitment and kindness.

I am deeply grateful to the Ministry of Higher Education (MOHE) Malaysia for funding this project through the Fundamental Research Grant Scheme (FRGS) (Grant No.: 9003-00336). In addition, I am thankful to the Malaysia Toray Science Foundation for presenting the Science & Technology Research Grant which financially aided my research project (Grant No.: 9002-00023).

I would like to express my heartfelt thanks to Dr. M.V.Venkatashamy Reddy from Department of Physics, National University of Singapore (NUS) for allowing me

to utilize the facilities in the Advanced Battery Lab. I would like to thank Mr. Shaikshavali Petnikota, Visiting Scholar at NUS for his patience guidance in fabricating coin cell batteries and data analyses.

On top of that, I was overwhelmed with gratitude for the support, encouragement, tolerance and love from my family, giving me the strength to complete my research project.

© This item is protected by original copyright

## TABLE OF CONTENTS

	<b>PAGE</b>
<b>THESIS DECLARATION</b>	i
<b>ACKNOWLEDGEMENTS</b>	ii
<b>TABLE OF CONTENTS</b>	iv
<b>LIST OF TABLES</b>	vii
<b>LIST OF FIGURES</b>	viii
<b>LIST OF ABBREVIATIONS</b>	xiv
<b>LIST OF SYMBOLS</b>	xv
<b>LIST OF EQUATIONS</b>	xvi
<b>ABSTRAK</b>	xvii
<b>ABSTRACT</b>	xviii
<b>CHAPTER 1 INTRODUCTION</b>	
1.1 Background	1
1.1.1 Lithium-ion batteries	2
1.1.2 Components of lithium ion batteries	4
1.2 Problem Statement	8
1.3 Objectives	10
1.4 Scope of Study	10

## CHAPTER 2 LITERATURE REVIEW

2.1	Crystal structures of cathode materials	12
2.2	Cathode materials with olivine structure	13
2.3	Cathode materials with spinel structure	14
2.4	Cathode materials with $\alpha$ -NaFeO <sub>2</sub> layered rock salt structure	15
2.4.1	Layered LiCoO <sub>2</sub> compound	15
2.4.2	Layered LiNiO <sub>2</sub> compound	18
2.4.3	Layered Nickel-Oxide, LiNi <sub>1-x</sub> M <sub>x</sub> O <sub>2</sub>	21
2.4.4	Lithium Nickel-Manganese-Cobalt Oxide LiNi <sub>1/3</sub> Mn <sub>1/3</sub> Co <sub>1/3</sub> O <sub>2</sub>	26
2.4.5	Lithium Nickel-Manganese-Cobalt Oxide LiNi <sub>x</sub> Mn <sub>y</sub> Co <sub>z</sub> O <sub>2</sub>	29
2.5	Possible oxygen non-stoichiometry in layered rock salt structures	38

## CHAPTER 3 RESEARCH METHODOLOGY

3.1	Materials synthesis	41
3.2	Materials characterisation / instrumentation	43
3.2.1	X-ray diffraction, indexing and refinement	43
3.2.2	Battery Testing	47

## CHAPTER 4 RESULTS AND DISCUSSION

4.1	Introduction	50
4.2	XRD analysis	51
4.2.1	XRD analysis of LiNi <sub>1/3</sub> Mn <sub>1/3</sub> Co <sub>1/3</sub> O <sub>2</sub>	51
4.2.2	XRD analysis of Li[(Ni <sub>0.5</sub> Mn <sub>0.5</sub> ) <sub>1-x</sub> Co <sub>x</sub> ]O <sub>2</sub> ( $x = 0.20, 0.15, 0.10, 0.05$ and $0$ )	52
4.2.3	XRD analysis of LiNi <sub>0.4</sub> Mn <sub>0.4</sub> Co <sub>0.2</sub> O <sub>2</sub> synthesised in oxygen as a function of temperature	55
4.2.4	XRD analysis of LiNi <sub>0.4</sub> Mn <sub>0.4</sub> Co <sub>0.2</sub> O <sub>2</sub> synthesised in air as a function of temperature	57
4.3	Structural analysis using Rietveld refinement	60
4.3.1	Lattice parameters and interlayer mixing of LiNi <sub>1/3</sub> Mn <sub>1/3</sub> Co <sub>1/3</sub> O <sub>2</sub> determined from Rietveld refinements	66

4.3.2	Lattice parameters and interlayer mixing of $\text{Li}[(\text{Ni}_{0.5}\text{Mn}_{0.5})_{1-x}\text{Co}_x]\text{O}_2$ composition ( $x = 0.20, 0.15, 0.10, 0.05$ and $0$ ) determined from Rietveld refinements	68
4.3.3	Lattice parameters and interlayer mixing of $\text{LiNi}_{0.4}\text{Mn}_{0.4}\text{Co}_{0.2}\text{O}_2$ synthesised in oxygen determined from Rietveld refinements	74
4.3.4	Lattice parameters and interlayer mixing of $\text{LiNi}_{0.4}\text{Mn}_{0.4}\text{Co}_{0.2}\text{O}_2$ synthesised in air determined from Rietveld refinements	80
4.4	Electrochemical analysis	85
4.4.1	Cyclic voltammetry and galvanostatic cycling of $\text{LiNi}_{1/3}\text{Mn}_{1/3}\text{Co}_{1/3}\text{O}_2$	85
4.4.2	Cyclic voltammetry and galvanostatic cycling of $\text{LiNi}_{0.4}\text{Mn}_{0.4}\text{Co}_{0.2}\text{O}_2$	88
<b>CHAPTER 5 CONCLUSIONS AND RECOMMENDATIONS</b>		
5.1	Summary	98
5.2	Recommendations for future work	99
5.3	Commercialisation potential	100
<b>REFERENCES</b>		
<b>APPENDIX A</b>		
<b>LIST OF PUBLICATIONS</b>		
<b>LIST OF AWARDS</b>		

## LIST OF TABLES

NO.		PAGE
1.1	Comparison data among various cathode materials for lithium ion- battery.	9
2.1	Hexagonal lattice parameter and percentage of Ni and Mn in Li layer (determined by Rietveld Analysis) of $\text{LiNi}_{1-x}\text{Mn}_x\text{O}_2$ prepared in $\text{O}_2$ .	23
2.2	Metal ion occupation for $\text{LiNi}_{1-y-z}\text{Mn}_y\text{Co}_z\text{O}_2$ from Rietveld refinement.	35
4.1	Starting model for structure refinement of $\text{LiCoO}_2$ (ICSD #51182).	61
4.2	Structural data for $\text{LiCoO}_2$ powder synthesised at $900\text{ }^\circ\text{C}$ for 12 hours obtained from Rietveld refinement.	63
4.3	Structural data for $\text{LiCoO}_2$ powder synthesised at $900\text{ }^\circ\text{C}$ for 12 hours using different $U_{\text{iso}}$ values for oxygen.	64
4.4	Final structural data using the obtained $U_{\text{iso}}$ values for the $\text{LiCoO}_2$ synthesised at $900\text{ }^\circ\text{C}$ in air for 12 hours.	65
4.5	Refined structural data for the $\text{LiNi}_{1/3}\text{Mn}_{1/3}\text{Co}_{1/3}\text{O}_2$ synthesised at $900$ and $950\text{ }^\circ\text{C}$ in oxygen for 12 hours.	66
4.6	Comparison of lattice parameters for the $\text{Li}[(\text{Ni}_{0.5}\text{Mn}_{0.5})_{1-x}\text{Co}_x]\text{O}_2$ powders ( $x = 0.20, 0.15, 0.10, 0.05$ and $0$ ) synthesised at $950\text{ }^\circ\text{C}$ in oxygen for 12 hours.	69
4.7	Comparison of lattice parameters of the $\text{LiNi}_{0.4}\text{Mn}_{0.4}\text{Co}_{0.2}\text{O}_2$ powders synthesis between $800 - 950\text{ }^\circ\text{C}$ in oxygen.	75
4.8	Comparison of lattice parameters of the $\text{LiNi}_{0.4}\text{Mn}_{0.4}\text{Co}_{0.2}\text{O}_2$ powders synthesised between $800 - 950\text{ }^\circ\text{C}$ in air.	80
A.1	Example of calculation of weight needed to prepare 3g of $\text{LiNi}_{1/3}\text{Mn}_{1/3}\text{Co}_{1/3}\text{O}_2$ sample.	107



## LIST OF FIGURES

NO.		PAGE
1.1	Diagram of the movements of lithium ions and electrons during charging and discharging.	4
2.1	Olivine structure of $\text{LiFePO}_4$ .	14
2.2	Spinel structure of $\text{LiMn}_2\text{O}_4$ .	15
2.3	$\text{LiMO}_2$ (M = most transition metals, such as Co, Ni, Mn, Cr, etc.) with $\alpha$ - $\text{NaFeO}_2$ type structure.	16
2.4	A typical XRD pattern of commercially available $\text{LiCoO}_2$ .	16
2.5	(a) Charge/discharge curves of $\text{Li/LiCoO}_2$ cells. (b) Variations in the discharge capacity with cycle numbers.	17
2.6	XRD pattern of $\text{LiCo}_{1-x}\text{Al}_x\text{O}_2$ ( $x=0, 0.1, 0.2$ and $0.3$ ) powders calcined at $900\text{ }^\circ\text{C}$ for 24 hours in air.	18
2.7	XRD pattern of $\text{LiNiO}_2$ synthesised at $750\text{ }^\circ\text{C}$ in oxygen with excess Li (Li:Ni=1.05:1).	20
2.8	Charge-discharge profile of $\text{LiNiO}_2$ synthesised at $750\text{ }^\circ\text{C}$ in oxygen with excess Li (Li:Ni=1.05:1).	20
2.9	XRD pattern of $\text{LiNi}_{1-x}\text{Ti}_x\text{O}_2$ ( $0.025 \leq x \leq 0.2$ ) obtained by $750\text{ }^\circ\text{C}$ for 30 h.	21
2.10	Cycling performance $\text{LiNi}_{1-x}\text{Ti}_x\text{O}_2$ ( $0.025 \leq x \leq 0.2$ ). The data was taken with a current density of $0.2\text{ mA cm}^{-2}$ .	22
2.11	Cycling performance of $\text{LiNi}_{1-x}\text{Mn}_x\text{O}_2$ ( $x=0 - 0.2$ ) electrode.	24
2.12	Initial charge-discharge curves of $\text{LiNi}_{1-x}\text{Mn}_x\text{O}_2$ ( $x=0 - 0.3$ ) prepared in $\text{O}_2$ .	24
2.13	(top) Cyclic voltammogram of $\text{LiNi}_{0.5}\text{Mn}_{0.5}\text{O}_2$ at $50\text{ }\mu\text{V s}^{-1}$ for calcinations temperatures of $450, 600$ and $700\text{ }^\circ\text{C}$ ( $1^{\text{st}}$ cycle). (bottom) Cycling stability of $\text{LiNi}_{0.5}\text{Mn}_{0.5}\text{O}_2$ for calcinations temperatures of $450, 600$ and $700\text{ }^\circ\text{C}$ .	25
2.14	XRD patterns for $\text{LiNi}_{1/3}\text{Mn}_{1/3}\text{Co}_{1/3}\text{O}_2$ synthesised by different methods.	26

2.15	(left) Initial charge-discharge curves of $\text{LiNi}_{1/3}\text{Mn}_{1/3}\text{Co}_{1/3}\text{O}_2$ synthesised by different methods at a current density of $20 \text{ mA g}^{-1}$ in the voltage range of 3 – 4.5 V. (right) Cycling performances $\text{LiNi}_{1/3}\text{Mn}_{1/3}\text{Co}_{1/3}\text{O}_2$ synthesised by different methods.	27
2.16	Enlarged logarithmic plot of $\text{LiNi}_{1/3}\text{Mn}_{1/3}\text{Co}_{1/3}\text{O}_2$ calcined at different temperatures 1000-1150 °C (Fujii <i>et al.</i> , 2007).	28
2.17	(a) Charge and discharge curves and (b) cycle performances of Li/ $\text{LiNi}_{1/3}\text{Mn}_{1/3}\text{Co}_{1/3}\text{O}_2$ cells operated at $0.4 \text{ mA cm}^{-2}$ in the voltage range of 2.5–4.3 V at 23 °C.	28
2.18	Variation in lattice parameters of as-synthesised $\text{Li}[\text{Ni}_{0.4}\text{Co}_x\text{Mn}_{0.6-x}]\text{O}_2$ ( $x= 0.1-0.4$ ). The calculated values were obtained as a result of Rietveld refinements.	30
2.19	Initial charge-discharge curves of Li/Li $[\text{Ni}_{0.4}\text{Co}_x\text{Mn}_{0.6-x}]\text{O}_2$ ( $x = 0.1-0.4$ ).	30
2.20	Specific discharge capacities of $\text{Li}[\text{Ni}_{0.4}\text{Co}_x\text{Mn}_{0.6-x}]\text{O}_2$ ( $x = 0.1-0.4$ ). The applied current density across the positive electrode was $20 \text{ mA g}^{-1}$ at 30 °C in voltage range of 3.0–4.3 V.	31
2.21	XRD pattern of $\text{Li}[(\text{Ni}_{0.5}\text{Mn}_{0.5})_{1-x}\text{Co}_x]\text{O}_2$ ( $0 \leq x \leq 0.2$ ) synthesised at 950 °C for 10 hours in air. (a) $x= 0$ (b) $x= 0.05$ (c) $x= 0.10$ (d) $x= 0.15$ (e) $x= 0.20$ .	32
2.22	Variation of lattice parameters of $\text{Li}[(\text{Ni}_{0.5}\text{Mn}_{0.5})_{1-x}\text{Co}_x]\text{O}_2$ ( $0 \leq x \leq 0.2$ ) calculated by Rietveld refinements.	32
2.23	Initial charge and discharge curves of $\text{Li}[(\text{Ni}_{0.5}\text{Mn}_{0.5})_{1-x}\text{Co}_x]\text{O}_2$ ( $0 \leq x \leq 0.2$ ) by applying a current of $36 \text{ mA g}^{-1}$ (a) $x=0$ (b) $x= 0.05$ (c) $x= 0.10$ (d) $x= 0.15$ (e) $x= 0.20$ .	33
2.24	Rietveld refinement fit between experimental and calculated powder X-ray patterns for $\text{LiNi}_{0.4}\text{Mn}_{0.4}\text{Co}_{0.2}\text{O}_2$ .	35
2.25	XRD patterns of $\text{LiNi}_{0.4}\text{Mn}_{0.4}\text{Co}_{0.2}\text{O}_2$ obtained at temperature (a) 300 °C (b) 600 °C (c) 750 °C (3hrs) (d) 750 °C (12 hrs) and (e) 750 °C (24 hrs).	36
2.26	Initial charge-discharge curves of for Li/Li $\text{Ni}_{0.4}\text{Mn}_{0.4}\text{Co}_{0.2}\text{O}_2$ cell cycled in the voltage range of 3.0-4.2 V at a current density of $0.2 \text{ mA cm}^{-2}$ .	36

2.27	TG data in air for $\text{Li}_2\text{MnO}_{3-\delta}$ samples (a) in high oxygen pressure at 120 atm $\text{O}_2$ , 700 °C for 3 h, (b) prepared at 900 °C and slow-cooled in air, (c) quenched from 1000 °C, and (d) quenched from 1100 °C. All cooling curves for (a)–(d) were similar (←). Data in (e) are for a sample that was heated in air and cooled from 1000 °C in $\text{N}_2$ . It is assumed that sample (a) had stoichiometry $\delta = 0$ at 25 °C and that all samples have the same $\delta$ value when heated in air at 1000 °C.	39
2.28	TG data for samples heated and cooled sequentially in $\text{O}_2$ , air, and $\text{N}_2$ .	40
3.1	Flow chart showing various steps involved in synthesising and characterising of $\text{Li}[(\text{Ni}_{0.5}\text{Mn}_{0.5})_{1-x}\text{Co}_x]\text{O}_2$ ( $x = 0.33, 0.20, 0.15, 0.10, 0.05, 0$ ) compound.	42
3.2	Flow chart showing steps to prepare cathode electrode for coin cell battery fabrication.	48
3.3	Battery assembly sequence.	48
4.1	The composition of $\text{Li}[(\text{Ni}_{0.5}\text{Mn}_{0.5})_{1-x}\text{Co}_x]\text{O}_2$ ( $x = 0.33, 0.20, 0.15, 0.10, 0.05, \text{ and } 0$ ) within the ternary triangle of $\text{LiCoO}_2$ - $\text{LiNiO}_2$ - $\text{LiMnO}_2$ .	51
4.2	XRD pattern for $\text{LiNi}_{1/3}\text{Mn}_{1/3}\text{Co}_{1/3}\text{O}_2$ synthesised at 900 and 950 °C in oxygen for 12 hours.	52
4.3	(a) XRD pattern as a function of $x$ for $\text{Li}[(\text{Ni}_{0.5}\text{Mn}_{0.5})_{1-x}\text{Co}_x]\text{O}_2$ powders ( $x = 0.20, 0.15, 0.10, 0.05$ and 0) synthesised at 950 °C in oxygen for 12 hours. (b) Enlarged region for $2\theta =$ around 36 ° and around 44 °.	53
4.4	Enlarged XRD pattern as a function of $x$ for $\text{Li}[(\text{Ni}_{0.5}\text{Mn}_{0.5})_{1-x}\text{Co}_x]\text{O}_2$ powders ( $x = 0.20, 0.15, 0.10, 0.05$ and 0) synthesised at 950 °C in oxygen for 12 hours (a) $2\theta = 17^\circ$ – $20^\circ$ (b) $2\theta = 42^\circ$ – $47^\circ$ .	55
4.5	XRD pattern as a function of temperature for $\text{LiNi}_{0.4}\text{Mn}_{0.4}\text{Co}_{0.2}\text{O}_2$ powder synthesized between 800 – 950 °C in oxygen for 12 hours.	56
4.6	Enlarged XRD pattern as a function of temperature for $\text{LiNi}_{0.4}\text{Mn}_{0.4}\text{Co}_{0.2}\text{O}_2$ powders synthesised in oxygen for 12 hours (a) $2\theta = 17^\circ$ – $20^\circ$ (b) $2\theta = 42^\circ$ – $47^\circ$ .	57
4.7	XRD pattern as a function of temperature for $\text{LiNi}_{0.4}\text{Mn}_{0.4}\text{Co}_{0.2}\text{O}_2$ powder synthesized between 800 – 950 °C in air for 12 hours.	58

4.8	Enlarged XRD pattern as a function of temperature for $\text{LiNi}_{0.4}\text{Mn}_{0.4}\text{Co}_{0.2}\text{O}_2$ powders synthesised in air for 12 hours (a) $2\theta = 17^\circ - 20^\circ$ (b) $2\theta = 42^\circ - 47^\circ$ .	59
4.9	Indexed XRD pattern for $\text{LiCoO}_2$ heated at $900^\circ\text{C}$ in air for 12 hours.	60
4.10	Rietveld plot of the $\text{LiCoO}_2$ powder synthesised at $900^\circ\text{C}$ in air for 12 hours.	65
4.11	Rietveld plot of the $\text{LiNi}_{1/3}\text{Mn}_{1/3}\text{Co}_{1/3}\text{O}_2$ synthesised at $900^\circ\text{C}$ in oxygen for 12 hours.	67
4.12	Rietveld plot of the $\text{LiNi}_{1/3}\text{Mn}_{1/3}\text{Co}_{1/3}\text{O}_2$ synthesised at $950^\circ\text{C}$ in oxygen for 12 hours.	67
4.13	Variations of the lattice $a$ as a function of cobalt content $x$ at $950^\circ\text{C}$ .	69
4.14	Variations of the lattice $c$ as a function of cobalt content $x$ at $950^\circ\text{C}$ .	70
4.15	Variations of the unit cell volume as a function of cobalt content $x$ at $950^\circ\text{C}$ .	70
4.16	Variations of occupancy of Ni on Li-site from GSAS refinement as a function of cobalt content $x$ at $950^\circ\text{C}$ .	71
4.17	Rietveld plot of the $\text{Li}[(\text{Ni}_{0.5}\text{Mn}_{0.5})_{1-x}\text{Co}_x]\text{O}_2$ where $x=0.2$ synthesised at $950^\circ\text{C}$ in oxygen for 12 hours.	72
4.18	Rietveld plot of the $\text{Li}[(\text{Ni}_{0.5}\text{Mn}_{0.5})_{1-x}\text{Co}_x]\text{O}_2$ where $x=0.15$ synthesised at $950^\circ\text{C}$ in oxygen for 12 hours.	72
4.19	Rietveld plot of the $\text{Li}[(\text{Ni}_{0.5}\text{Mn}_{0.5})_{1-x}\text{Co}_x]\text{O}_2$ where $x=0.10$ synthesised at $950^\circ\text{C}$ in oxygen for 12 hours.	73
4.20	Rietveld plot of the $\text{Li}[(\text{Ni}_{0.5}\text{Mn}_{0.5})_{1-x}\text{Co}_x]\text{O}_2$ where $x=0.05$ synthesised at $950^\circ\text{C}$ in oxygen for 12 hours.	73
4.21	Rietveld plot of the $\text{Li}[(\text{Ni}_{0.5}\text{Mn}_{0.5})_{1-x}\text{Co}_x]\text{O}_2$ where $x=0$ synthesised at $950^\circ\text{C}$ in oxygen for 12 hours.	74
4.22	Variations of the lattice $a$ as a function of temperature for $\text{LiNi}_{0.4}\text{Mn}_{0.4}\text{Co}_{0.2}\text{O}_2$ powders synthesised between $800 - 950^\circ\text{C}$ in oxygen.	76
4.23	Variations of the lattice $c$ as a function of temperature for $\text{LiNi}_{0.4}\text{Mn}_{0.4}\text{Co}_{0.2}\text{O}_2$ powders synthesised between $800 - 950^\circ\text{C}$ in oxygen.	76

4.24	Variations of the unit cell volume as a function of temperature for $\text{LiNi}_{0.4}\text{Mn}_{0.4}\text{Co}_{0.2}\text{O}_2$ powders synthesised between 800 - 950 °C in oxygen.	77
4.25	Variations of occupancy of Ni on Li-site from GSAS refinement as a function of temperature for $\text{LiNi}_{0.4}\text{Mn}_{0.4}\text{Co}_{0.2}\text{O}_2$ powders synthesised between 800 - 950 °C in oxygen.	77
4.26	Rietveld plot of the $\text{LiNi}_{0.4}\text{Mn}_{0.4}\text{Co}_{0.2}\text{O}_2$ powders synthesised at 800 °C in oxygen.	78
4.27	Rietveld plot of the $\text{LiNi}_{0.4}\text{Mn}_{0.4}\text{Co}_{0.2}\text{O}_2$ powders synthesised at 850 °C in oxygen.	79
4.28	Rietveld plot of the $\text{LiNi}_{0.4}\text{Mn}_{0.4}\text{Co}_{0.2}\text{O}_2$ powders synthesised at 900 °C in oxygen.	79
4.29	Variations of the lattice $a$ as a function of temperature for $\text{LiNi}_{0.4}\text{Mn}_{0.4}\text{Co}_{0.2}\text{O}_2$ powders synthesised between 800 - 950 °C in air.	81
4.30	Variations of the lattice $c$ as a function of temperature for $\text{LiNi}_{0.4}\text{Mn}_{0.4}\text{Co}_{0.2}\text{O}_2$ powders synthesised between 800 - 950 °C in air.	81
4.31	Variations of the unit cell volume as a function of temperature for $\text{LiNi}_{0.4}\text{Mn}_{0.4}\text{Co}_{0.2}\text{O}_2$ powders synthesised between 800 - 950 °C in air.	82
4.32	Variations of occupancy of Ni on Li-site from GSAS refinement as a function of temperature for $\text{LiNi}_{0.4}\text{Mn}_{0.4}\text{Co}_{0.2}\text{O}_2$ powders synthesised between 800 - 950 °C in air.	82
4.33	Rietveld plot of the $\text{LiNi}_{0.4}\text{Mn}_{0.4}\text{Co}_{0.2}\text{O}_2$ powders synthesised at 800 °C in air.	83
4.34	Rietveld plot of the $\text{LiNi}_{0.4}\text{Mn}_{0.4}\text{Co}_{0.2}\text{O}_2$ powders synthesised at 850 °C in air.	84
4.35	Rietveld plot of the $\text{LiNi}_{0.4}\text{Mn}_{0.4}\text{Co}_{0.2}\text{O}_2$ powders synthesised at 900 °C in air.	84
4.36	Rietveld plot of the $\text{LiNi}_{0.4}\text{Mn}_{0.4}\text{Co}_{0.2}\text{O}_2$ powders synthesised at 950 °C in air.	85
4.37	Cyclic voltammogram at a sweep rate of $0.058 \text{ mV s}^{-1}$ of $\text{LiNi}_{1/3}\text{Mn}_{1/3}\text{Co}_{1/3}\text{O}_2$ synthesised at 950 °C in oxygen for 12 hours.	86

4.38	1 <sup>st</sup> , 10 <sup>th</sup> , 20 <sup>th</sup> , 30 <sup>th</sup> and 45 <sup>th</sup> charge and discharge curves of LiNi <sub>1/3</sub> Mn <sub>1/3</sub> Co <sub>1/3</sub> O <sub>2</sub> synthesised at 950 °C in oxygen for 12 hours.	87
4.39	Cycling performance of LiNi <sub>1/3</sub> Mn <sub>1/3</sub> Co <sub>1/3</sub> O <sub>2</sub> synthesised at 950 °C in oxygen for 12 hours.	88
4.40	Cyclic voltammogram at a sweep rate of 0.058 mV s <sup>-1</sup> of LiNi <sub>0.4</sub> Mn <sub>0.4</sub> Co <sub>0.2</sub> O <sub>2</sub> synthesised at 950 °C in oxygen for 12 hours.	90
4.41	Cyclic voltammogram at a sweep rate of 0.058 mV s <sup>-1</sup> of LiNi <sub>0.4</sub> Mn <sub>0.4</sub> Co <sub>0.2</sub> O <sub>2</sub> synthesised at 950 °C in air for 12 hours.	90
4.42	Cyclic voltammogram at a sweep rate of 0.058 mV s <sup>-1</sup> of LiNi <sub>0.4</sub> Mn <sub>0.4</sub> Co <sub>0.2</sub> O <sub>2</sub> synthesised at 900 °C in oxygen for 12 hours.	91
4.43	1 <sup>st</sup> , 10 <sup>th</sup> , 20 <sup>th</sup> , 30 <sup>th</sup> and 45 <sup>th</sup> charge and discharge curves of LiNi <sub>0.4</sub> Mn <sub>0.4</sub> Co <sub>0.2</sub> O <sub>2</sub> synthesised at 950 °C in oxygen for 12 hours.	92
4.44	Cycling performance of LiNi <sub>0.4</sub> Mn <sub>0.4</sub> Co <sub>0.2</sub> O <sub>2</sub> synthesised at 950 °C in oxygen for 12 hours.	92
4.45	1 <sup>st</sup> , 10 <sup>th</sup> , 20 <sup>th</sup> , 30 <sup>th</sup> and 45 <sup>th</sup> charge and discharge curves of LiNi <sub>0.4</sub> Mn <sub>0.4</sub> Co <sub>0.2</sub> O <sub>2</sub> synthesised at 950 °C in air for 12 hours.	93
4.46	Cycling performance of LiNi <sub>0.4</sub> Mn <sub>0.4</sub> Co <sub>0.2</sub> O <sub>2</sub> synthesised at 950 °C in air for 12 hours.	94
4.47	1 <sup>st</sup> , 10 <sup>th</sup> , 20 <sup>th</sup> and 25 <sup>th</sup> charge and discharge curves of LiNi <sub>0.4</sub> Mn <sub>0.4</sub> Co <sub>0.2</sub> O <sub>2</sub> synthesised at 900 °C in oxygen for 12 hours.	95
4.48	Cycling performance of LiNi <sub>0.4</sub> Mn <sub>0.4</sub> Co <sub>0.2</sub> O <sub>2</sub> synthesised at 900 °C in oxygen for 12 hours.	95
4.49	Comparisons of discharge capacities between LiNi <sub>0.4</sub> Mn <sub>0.4</sub> Co <sub>0.2</sub> O <sub>2</sub> synthesised at different conditions and LiNi <sub>1/3</sub> Mn <sub>1/3</sub> Co <sub>1/3</sub> O <sub>2</sub> .	97

## LIST OF ABBREVIATIONS

Co	Cobalt
DMC	Dimethyl carbonate
EC	Ethylene carbonate
EVs	Electric vehicles
GSAS	General Structure Analysis System
Li	Lithium
Li[PF <sub>3</sub> (C <sub>2</sub> F <sub>5</sub> ) <sub>3</sub> ]	Fluoroalkylphosphates
Li <sub>15</sub> Si <sub>4</sub>	Lithium silicides
Li <sub>2</sub> MnO <sub>3</sub>	Lithium manganese oxide
LiCoO <sub>2</sub>	Lithium cobalt oxide
LiFePO <sub>4</sub>	Lithium iron phosphate
LiNiO <sub>2</sub>	Lithium nickel oxide
LiPF <sub>6</sub>	Lithium hexafluorophosphate
Mn	Manganese
Ni	Nickel
Ni-Cd	Nickel cadmium
Ni-MH	Nickel-metal hydride
NMP	N-methylpyrrolidone
O <sub>2</sub>	Oxygen
PVDF	Polyvinylidene difluoride binder
TGA	Thermogravimetric analysis
XRD	X-ray Diffraction

## LIST OF SYMBOLS

$2\theta$	Diffraction angle
$\lambda$	wavelength
$\chi^2$	Reduced Chi <sup>2</sup>

© This item is protected by original copyright



## LIST OF EQUATIONS

NO.		PAGE
3.1	$2d \sin \theta = n \lambda$	43
3.2	Gaussian component: $\text{FWHM} = (U \tan^2 \theta + V \tan \theta + W)^{1/2}$	45
3.3	Lorentzian component: $\text{FWHM} = (X \tan \theta + Y / \cos \theta)^{1/2}$	45
3.4	$\chi^2 = \left( \frac{R_{wp}}{R_{exp}} \right)^2$	46

© This item is protected by original copyright

## Pencampuran antara Lapisan dalam Bahan Katod Litium Nikel Mangan Kobalt Oksida untuk Bateri Litium Cas Semula

### ABSTRAK

Komposisi  $\text{LiNi}_{1/3}\text{Mn}_{1/3}\text{Co}_{1/3}\text{O}_2$  dan analoginya  $\text{Li}[(\text{Ni}_{0.5}\text{Mn}_{0.5})_{1-x}\text{Co}_x]\text{O}_2$  telah disintesis menggunakan kaedah tindak balas keadaan pepejal konvensional untuk menilai kesan pengurangan kandungan kobalt dalam bahan katod bateri yang berstruktur garam batu berlapis. Analisis struktur menggunakan kaedah penyaringan Rietveld menggunakan data XRD konvensional telah mendedahkan bahawa kandungan kobalt adalah saling berhubungkait dengan kestabilan struktur bahannya. Had larutan pepejal bagi sampel fasa-tulen yang disintesis ialah sekitar  $x \geq 0.2$  untuk  $\text{Li}[(\text{Ni}_{0.5}\text{Mn}_{0.5})_{1-x}\text{Co}_x]\text{O}_2$ . Jumlah pencampuran antara lapisan telah meningkat bagi sampel yang mengandungi 20% atau kurang kandungan kobalt. Keputusan menunjukkan jumlah pencampuran antara lapisan paling minima yang boleh dicapai ialah lebih kurang 3.8% bagi komposisi  $\text{LiNi}_{0.4}\text{Mn}_{0.4}\text{Co}_{0.2}\text{O}_2$  yang disintesis pada suhu  $950^\circ\text{C}$  dalam oksigen berbanding dengan  $\text{LiNi}_{1/3}\text{Mn}_{1/3}\text{Co}_{1/3}\text{O}_2$  iaitu sekitar 2%. Walau bagaimanapun, jumlah pencampuran antara lapisan berbeza-beza mengikut perubahan suhu dan keadaan sintesis. Kajian sistematik telah dijalankan untuk mengoptimumkan parameter penyaringan dan mengesahkan model struktur berdasarkan  $\text{LiCoO}_2$  sebagai piawaian. Di samping itu, kapasiti cas dan discas permulaan semasa kitaran bateri untuk  $\text{LiNi}_{0.4}\text{Mn}_{0.4}\text{Co}_{0.2}\text{O}_2$  adalah agak tinggi dengan mencatat masing-masing ialah  $\sim 323 \text{ mAh g}^{-1}$  dan  $\sim 229 \text{ mAh g}^{-1}$ . Namun begitu, ia mempunyai kehilangan kapasiti tidak boleh diubah yang tinggi selepas beberapa kitaran yang mungkin disebabkan oleh ketidakstabilan struktur semasa cas dan discas.

## Interlayer Mixing in Lithium Nickel Manganese Cobalt Oxide Cathode Materials for Rechargeable Lithium Batteries

### ABSTRACT

Composition of  $\text{LiNi}_{1/3}\text{Mn}_{1/3}\text{Co}_{1/3}\text{O}_2$  and its analogous  $\text{Li}[(\text{Ni}_{0.5}\text{Mn}_{0.5})_{1-x}\text{Co}_x]\text{O}_2$  were prepared by conventional solid state method to evaluate the effect of reducing cobalt contents to the layered rock salt-type cathode materials. Structural analysis using Rietveld refinement of conventional XRD data revealed that the amount of cobalt contents is highly correlated to their structural stability. Solid solution limit for phase-pure samples that were prepared is about  $x \geq 0.2$  for  $\text{Li}[(\text{Ni}_{0.5}\text{Mn}_{0.5})_{1-x}\text{Co}_x]\text{O}_2$ . The amount of interlayer mixing increased for samples contain 20% or less cobalt contents. The results showed that the minimum amount of interlayer mixing that could be achieved is about 3.8% for the composition of  $\text{LiNi}_{0.4}\text{Mn}_{0.4}\text{Co}_{0.2}\text{O}_2$  that was prepared at 950 °C in oxygen compared to  $\text{LiNi}_{1/3}\text{Mn}_{1/3}\text{Co}_{1/3}\text{O}_2$  which is about 2%. However, the amount of interlayer mixing varies as a function of temperatures and conditions. Systematic investigation have been done to optimize refinement parameters and to validate structural model based on  $\text{LiCoO}_2$  as a standard. On the other hand, the initial charge and discharge capacities during battery cycling for  $\text{LiNi}_{0.4}\text{Mn}_{0.4}\text{Co}_{0.2}\text{O}_2$  is relatively high which recorded  $\sim 323 \text{ mAh g}^{-1}$  and  $\sim 229 \text{ mAh g}^{-1}$  respectively. But it has high irreversible capacity loss after a few cycles that are probably due to structural instability during charge and discharge.

© This item is protected by copyright. All rights reserved.

# CHAPTER 1

## INTRODUCTION

### 1.1 Background

Nowadays, batteries are the main source of power for portable electronic devices and also for automobile starting and ignition. The increasing global energy demands and the arising of environmental concerns have caused batteries to be intensively pursued for a widespread hybrid electric vehicle (HEV) and plug-in hybrid electric vehicle (PHEV) applications. The batteries performances are affected by the materials used and the engineering involved in fabricating them (Arumugam, 2010).

Batteries are commonly classified into primary and secondary batteries. Primary batteries cannot be electrically charged because there are irreversible chemical reactions involved in the electrode materials (Arumugam, 2010). However, they provide good storage characteristics and high energy density. They existed in many forms, for instances, lithium-thionyl chloride, lithium-carbon monofluoride and lithium-manganese dioxide batteries. These batteries have been commercialised for more than 30 years. Other batteries such as carbon-zinc, alkaline-manganese, zinc-air, and silver oxide-zinc batteries are used together with these batteries.

Secondary batteries which are opposed to primary batteries can be electrically charged, and these batteries can save costs and resources. For example, lithium-ion and nickel-metal hydride batteries have been produced, and are used with the other secondary batteries, such as lead-acid, nickel-cadmium and coin-type lithium secondary batteries. The diversity and the applications for conventional and new practical battery systems have been increasing for the last 30 years.

### **1.1.1 Lithium ion batteries**

Lithium-ion batteries which are in the family of rechargeable batteries are also well known as the most important energy storage device. They are lighter, can last for longer time and quicker to charge compared to their nickel-based relatives. The worldwide market for rechargeable lithium-ion batteries are now valued at 10 billion dollars per annum and is arising. Such rapid growth is mainly due to its higher energy density and better cycling performance than other energy storage devices. Recent demands on energy and environmental sustainability have further urged significant interest in a larger scale lithium-ion battery system for vehicles and grid load leveling (Choi, Wang, & Yang, 2011).

The lithium-ion batteries have a quite straightforward energy storage mechanism in which they store electrical energy in electrodes that are made of lithium-intercalation (or insertion) compounds with reduction and oxidation processes occurring simultaneously at the two electrodes (Choi, Wang, & Yang, 2011). Lithium-ion batteries usually consist of complex lithium oxides containing a transition metal oxide as the positive electrode (cathode) material, a carbon material as the negative electrode

(anode) material and organic solvent as electrolyte between these two electrodes (Nishio & Furukawa, 1999).

The lithium ion secondary battery (LIB) technology was initiated by Sony Corporation which brought out the lithium ion cells into the market first in the world in 1991. Some basic characteristics of LIB are as follows (Yoshio, 2000).

- a. high energy density (both gravimetric and volumetric),
- b. high operating voltage,
- c. no memory effect,
- d. high drain capability,
- e. quick charge acceptance,
- f. low self-discharge rate,
- g. wide temperature range of operation

When the cell is fabricated, it is in the discharge condition. When it is charged, both lithium ions and electrons move from the positive electrode to the negative electrode. The lithium ions move through the electrolyte whereas the electrons move through the external circuit during charging. Generally, the cells voltage will become higher as the potential of the cathode rises and that of anode is lowered during charging. When a load is connected between the positive and negative electrodes, the cell is discharged where the lithium ions and electrons move from the negative electrode to the positive electrode. Electrical energy is obtained as a result of the diffusion of lithium ions and electrons (Nishio & Furukawa, 1999). Fig. 1.1 illustrated the movements of lithium ions and electrons during charging and discharging. (Arumugam, 2010).

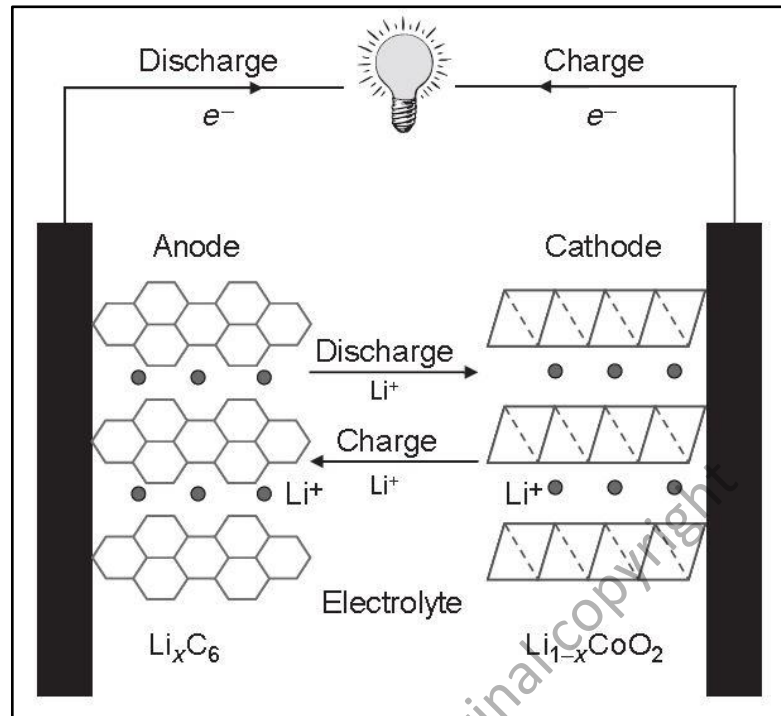


**Figure 1.1:** Diagram of the movements of lithium ions and electrons during charging and discharging (Arumugam, 2010).

### 1.1.2 Components of lithium ion batteries

As mention before, there are three main components in lithium ion batteries which include negative electrode (anode), electrolyte and positive electrode (cathode).

#### i. Negative electrode (anode)

In lithium ion battery, the anode is the negative electrode of a cell where oxidative chemical reactions occurred. During discharge, it releases electrons into the external circuit (Whittingham, 2004). There are a wide range of materials with potential and practical applications in the field of anode materials for lithium-ion batteries.

Initially, Li metals which have high energy density are used as anode. Since Li metals are very active, a passivating surface layer is formed on the lithium anode when Li reacts with the electrolyte. This protection layer prevents further reaction because it is an electronic insulator and a lithium ion conductor (Wakihara & Yamamoto, 1998). The usage of Li metal and alloys as the anode materials were until the 1980s due to safety issue (Aifantis & Hackney, 2010). However, lithium alloy anode materials have been reviewed focusing on the lithium alloying in Group IV and V elements and their composites from mechanistic aspects of (Park *et al.*, 2010).

In the past, carbon that is low cost, easily available and possible to be modified made it hard to be replaced by other anode material. Many researchers have been studied in depth on the alternative forms of carbon materials and their corresponding reaction mechanism, surface effects, new nano-materials and so on (Alcántara *et al.*, 2011). After year 1991 in which Sony Energytec Inc. first commercialised the lithium ion battery, graphite has become the standard anode for lithium ion batteries. It has a specific capacity of 300 mAh g<sup>-1</sup> (Kendrick & Slater, 2011) However, the theoretical capacity (372 mAh g<sup>-1</sup>) is poor compared with the charge density of lithium (3,862 mAh g<sup>-1</sup>). Hence, novel graphite varieties and carbon nanotubes have been proposed to improve the capacity but they encountered with high processing costs (Wakihara & Yamamoto, 1998).

Apart from carbonaceous material, there are a few materials which have drawn interests of many researchers. These include transition metal oxides, nitrides, phosphides, antimonides, silicon and silicon compound, last but not least, tin and tin alloy compounds.